Astronomy & Astrophysics manuscript no. 37679
June 9, 2020

Calibrating the surface brightness - color relation for late-type red giants stars in the visible domain using VEGA/CHARA interferometric observations

N. Nardetto[1], A. Salsi[1], D. Mourard[1], V. Hocdé[1], K. Perraut[2], A. Gallenne[1,3,4,5], A. Mérand[6], D. Graczyk[3,4], G. Pietrzynski[4], W. Gieren[3], P. Kervella[7], R. Ligi[8], A. Meilland[1], F. Morand[1], P. Stee[1], I. Tallon-Bosc[9], and T. ten Brummelaar[10,11]

[1] Université Côte d'Azur, Observatoire de la Côte d'Azur, CNRS, Laboratoire Lagrange, France
[2] Univ. Grenoble Alpes, CNRS, IPAG, 38000 Grenoble, France
[3] Departamento de Astronomía, Universidad de Concepción, Casilla 160-C, Concepción, Chile
[4] Nicolaus Copernicus Astronomical Center, Polish Academy of Sciences, ul. Bartycka 18, PL-00-716 Warszawa, Poland.
[5] Unidad Mixta Internacional Franco-Chilena de Astronomía (CNRS UMI 3386), Departamento de Astronomía, Universidad de Chile, Camino El Observatorio 1515, Las Condes, Santiago, Chile
[6] European Southern Observatory, Alonso de Córdova 3107, Casilla 19001, Santiago 19, Chile
[7] LESIA (UMR 8109), Observatoire de Paris, PSL, CNRS, UPMC, Univ. Paris-Diderot, 5 place Jules Janssen, 92195 Meudon, France
[8] Osservatorio Astronomico di Brera, Via E. Bianchi 46, 23807 Merate, Italy.
[9] Université de Lyon, Université Lyon 1, Ecole Normale Supérieure de Lyon, CNRS, Centre de Recherche Astrophysique de Lyon UMR5574, F-69230, Saint-Genis-Laval, France
[10] Georgia State University, P.O. Box 3969, Atlanta GA 30302-3969, USA
[11] CHARA Array, Mount Wilson Observatory, 91023 Mount Wilson CA, USA

Received ... ; accepted ...

ABSTRACT

Context. The surface brightness - color relationship (SBCR) is a poweful tool for determining the angular diameter of stars from photometry. It was for instance used to derive the distance of eclipsing binaries in the Large Magellanic Cloud (LMC), which led to its distance determination with an accuracy of 1%.
Aims. We calibrate the SBCR for red giant stars in the $2.1 \leq V-K \leq 2.5$ color range using homogeneous VEGA/CHARA interferometric data secured in the visible domain, and compare it to the relation based on infrared interferometric observations, which were used to derive the distance to the LMC.
Methods. Observations of eight G-K giants were obtained with the VEGA/CHARA instrument. The derived limb-darkened angular diameters were combined with a homogeneous set of infrared magnitudes in order to constrain the SBCR.
Results. The average precision we obtain on the limb-darkened angular diameters of the eight stars in our sample is 2.4%. For the four stars in common observed by both VEGA/CHARA and PIONIER/VLTI, we find a 1σ agreement for the angular diameters. The SBCR we obtain in the visible has a dispersion of 0.04 magnitude and is consistent with the one derived in the infrared (0.018 magnitude).
Conclusions. The consistency of the infrared and visible angular diameters and SBCR reinforces the result of 1% precision and accuracy recently achieved on the distance of the LMC using the eclipsing-binary technique. It also indicates that it is possible to combine interferometric observations at different wavelengths when the SBCR is calibrated.

Key words. Techniques: interferometry – Stars: atmospheres – Stars: distances – (Stars:) binaries: eclipsing – Stars: late-type – stars: fundamental parameters

1. Introduction

In the era of precision cosmology, it is essential to determine the Hubble constant to an accuracy of 2% or better (Komatsu et al. 2011; Freedman & Madore 2010). Recently, Riess et al. (2019) achieved a 1.9% precision by relying on the distance to the Large Magellanic Cloud (LMC), which is the best anchor point for the cosmic distance scale (Schaefer 2008; Walker et al. 2012; Riess et al. 2016). Late-type eclipsing-binary systems provide the opportunity of measuring accurate distances by combining the linear diameter (derived from the light curve and velocimetry) and angular diameters (derived from a surface-brightness color relation, SBCR) of their components.

Based on the observation of some 35 million stars in the LMC for more than 20 years during the Optical Gravitational Lensing Experiment (OGLE) (Udalski et al. 2008), a few dozen extremely scarce long-period eclipsing sys-

tems composed of late-type clump giants were cataloged (Graczyk et al. 2011; Pawlak et al. 2016). In the course of the Araucaria project (Gieren et al. 2005), Pietrzyński et al. (2013) studied 8 systems and derived a distance to the LMC at the 2.2% level. This distance relied on the SBCR derived by Di Benedetto (2005) and thus was completely dominated by the error of 2% (or 0.03 magnitude) on this relation. Then, Laney et al. (2012) secured uniform and precise K-band photometry (precision of about $\simeq$0.01 mag) for a large sample of nearby very bright red giants located in a very well defined and quiet evolutionary phase of the core-helium burning (red clump). In addition, Gallenne et al. (2018) secured observations of 48 of these red-clump stars in the H band with the Precision Integrated Optics Near-infrared Imaging ExpeRiment (PIONIER, Le Bouquin et al. (2011)) installed at the Very Large Telescope Interferometer. These measurements allowed deriving an SBCR with an rms of 0.018 magnitude. This relation was used to derive the individual angular diameters of the 20 eclipsing binaries at the 0.8% precision level, which finally led to a distance of the LMC that is accurate to 1% (Pietrzyński et al. 2019).

The purpose of this paper is to calibrate the SBCR in the visible domain in order to compare it to the one derived in the H band. For this, we observed a subsample of eight stars in the visible domain with interferometry, using the Visible spEctroGraph and polArimeter (VEGA) beam combiner (Mourard et al. 2009, 2011) operating at the focus of The Center for High Angular Resolution Astronomy (CHARA) array (ten Brummelaar et al. 2005), which is located at the Mount Wilson Observatory. In Sect. 2 we describe the VEGA/CHARA interferometric observations and provide the limb-darkened angular diameters of the eight stars in our sample. Sect. 3 is dedicated to the calibration of the SBCR. The results are then discussed in Section 4, and we conclude in Section 5.

2. VEGA/CHARA observations of eight late-type stars

We selected eight late-type stars with existing infrared photometry by Laney et al. (2012), with a $(V-K)_0$ color index ranging from 2.12 to 2.43, which corresponds to the index that was used to derive the distance to the LMC (2.05-2.75). They are red giants stars (δ between -9^o to 12^o) with spectral types ranging from G8 to K2. They have a visual magnitude $m_{\rm V}$ ranging from 5.8 to 6.2, which is well below the limiting magnitude of VEGA. They are also bright in the K band (with $m_{\rm K} < 3.9$), which allows us to track the group delay simultaneously with the infrared CLIMB combiner (Sturmann et al. 2010). We observed our sample from 2013 July to 2014 October using different suitable telescopes available on the CHARA array. A summary of the observations is given in Table 1.

For these observations, we used the medium spectral resolution mode of VEGA ($R \simeq 5000$) and the standard VEGA pipeline in order to calibrate the squared visibilities in spectral bands of 15 or 20 nm (Mourard et al. 2009, 2011; Ligi et al. 2013). The integration time of our observations is of 500 seconds. For each calibrated visibility, the statistical and systematic calibration errors are given separately in Tab. B.1. The systematic uncertainty stems from the uncertainty on the calibrator diameter, which is given in Tab. 2. To perform the model fitting, we used a JMMC[1] tool, *LITpro* (Tallon-Bosc et al. 2008). The systematic and statistical errors are considered separately in the fitting procedure and are propagated until the final error on the surface brightness. In Fig. A.1 and A.2, the calibrated visibilities are plotted as a function of the spatial frequency together with the corresponding (u,v) coverage for each star. We fit these calibrated visibilities by a uniform disk, where the so-called uniform-disk angular diameter ($\theta_{\rm UD}$) is the only parameter. The results are given in Tab. 3. We then converted these $\theta_{\rm UD}$ diameters into limb-darkened ($\theta_{\rm LD}$) angular diameters. A common and convenient approach is to use a linear law for the continuum-intensity profile of the star, defined by $I(\cos(\alpha)) = 1 - u + u\cos(\alpha)$, where u is the linear limb-darkening coefficient of the star in the interferometric wavelength band of observation (Claret & Bloemen 2011). α is the angle between the normal of the star and the line of sight. The limb-darkened angular diameter is then calculated using $\theta_{\rm LD} = \theta_{\rm UD}\left[\frac{(1-\frac{u}{3})}{(1-\frac{7u}{15})}\right]^{\frac{1}{2}}$ (Han-

Table 1. Summary of the observing log. All the details are given in Tab. B.1. N corresponds to the number of visibility measurements for each star. The reference stars are also indicated (cf. Tab. 2).

star	telescope configurations	N	reference stars
HD11037	E1E2W2, W1W2S2	4	C1, C2
HD13468	E1E2W2, W1W2E2	7	C3
HD22798	E1E2W2, W1W2S2	4	C4
HD23526	E1E2W2, W1W2S2	9	C4
HD360	S1S2W2	7	C5, C6
HD40020	E1E2, W1W2	6	C7, C8
HD43023	E1E2W2, W1W2S2	7	C9, C10, C11, C12
HD5268	W2W1S2	2	C5, C6

Table 2. Reference stars and their parameters, including the spectral type, the visual magnitude ($m_{\rm V}$), and the predicted uniform-disk angular diameter (in mas) together with its corresponding uncertainty derived from the JMMC *SearchCal* software (Bonneau et al. 2006; Lafrasse et al. 2010). The uncertainties on the reference stars are about 7%, which is conservative.

	reference stars	spectral type	$m_{\rm V}$ [mag]	$\theta_{\rm UD}[R]$ [mas]
C1	HD18604	B6III	4.70	0.259 ± 0.018
C2	HD224926	B7III-IV	5.10	0.192 ± 0.014
C3	HD15633	A3V	6.01	0.252 ± 0.018
C4	HD23363	B7IV	5.25	0.201 ± 0.014
C5	HD219402	A2V	5.55	0.249 ± 0.018
C6	HD6530	A0V	5.58	0.234 ± 0.017
C7	HD34203	A0V	5.52	0.221 ± 0.016
C8	HD30034	F0V	5.38	0.407 ± 0.029
C9	HD43445	B9V	5.00	0.239 ± 0.017
C10	HD32249	B3IV	4.81	0.176 ± 0.012
C11	HD46487	B5IV/V	5.08	0.180 ± 0.013
C12	HD34863	B7/8V	5.28	0.181 ± 0.013

[1] http://www.jmmc.fr/

bury Brown et al. 1974). In the Claret tables, u is given as a function of the effective temperature $T_{\rm eff}$, the surface gravity $\log g$, the metallicity Z and the microturbulence velocity $V_{\rm t}$, in several photometric bands, including the R band ($\lambda_{\rm eff}$ = 670nm) and the I band ($\lambda_{\rm eff}$ = 856nm). The fundamental parameters of the stars are given in Tab. 4 together with the rounded values used as an input in the Claret tables. After they are extracted from these tables, the limb-darkened coefficients in the R and I bands were interpolated at the typical wavelength band of our observations, that is, 710 mn, in order to derive the corresponding linear limb-darkening coefficient ($u_{[710]}$). The resulting $u_{[710]}$ parameters are given in Tab. 3 together with the corresponding limb-darkened angular diameters. The reduced χ^2 ranges from 0.4 to 2.9.

Changing the effective temperature by 500 K and/or the surface gravity by 0.5 have an effect on the limb-darkening angular diameter of 1.3%. The grid in effective temperature has a step of 250 K, thus the largest error we can make on the temperature is 125 K, which corresponds to an additional uncertainty on the limb-darkened diameter of about 0.3%. However, the fact that the derived diameters are weakly sensitive to the input parameters of the limb-darkening law does not exclude that they might be sensitive to the limb-darkening law itself or to the method. We also tested the method by fitting the limb-darkened angular diameter with the *limb_linear* function of the *LITpro* tool, that is, by fixing the limb-darkening coefficient to its value indicated in Tab. 4. The derived limb-darkened angular diameters are 0.4 to 0.8% larger (except for HD 23526, for which we find 1.2%) than those indicated in Tab. 4 based on the approximate analytic conversion law. This bias is larger than what has been stated by Hanbury Brown et al. (1974), which is an approximation of $< 0.4\%$ if $u_{\rm R}$ ranges from 0.5 to 1.0. The uncertainties are strictly the same, however. For the limb-darkening law itself, we also used the dedicated SATLAS models by Neilson & Lester (2013a,b) to derive the limb-darkened diameters using the same input physical parameters as those indicated in Tab. 4. With this approach, we find diameters that are about 0.4% larger than the values presented in Tab. 3. These tests are interesting and should be considered with caution when a limb-darkened angular diameter is derived at the sub-percent level, but our statistical precision here is about 2.4% and the common analytical approach leads to a bias on our SBCR calibration at a far lower level than our statistical precision.

Our sample includes four stars that are in common with samples of Gallenne et al. (2018) and Pietrzyński et al. (2019): HD13468, HD23526, HD360, and HD40020. Their PIONIER/VLTI angular diameters are listed in Tab. 3. This is an interesting opportunity to compare the angular diameters derived from CHARA/VEGA and VLTI/PIONIER (see Fig. 1). We find that the CHARA/VEGA angular diameters are consistent within their uncertainties with those from VLTI/PIONIER. Visible (this work) and infrared (Gallenne et al. 2018) interferometric observations are thus in agreement, which means that the conversions from UD into LD angular diameters are at least consistent in the two wavelength domains (R and H) at the sub-percent level. Moreover, it indicates that there is negligible systematics on the instrumental point of view in the determination of the angular diameters. Both instruments might be biased in exactly the same way (for the four stars), but this is highly unlikely. The calibrators used in the VLTI/PIONIER analysis are giants with spectral types ranging from G8 to K2, which is significantly colder and more resolved than the calibrators we used in our analysis in the visible domain (Tab. 2). We therefore expect that the systematics on the squared visibilities (Tab. 2) that stem from the uncertainties on the calibrators are significantly lower in the visible than in the infrared.

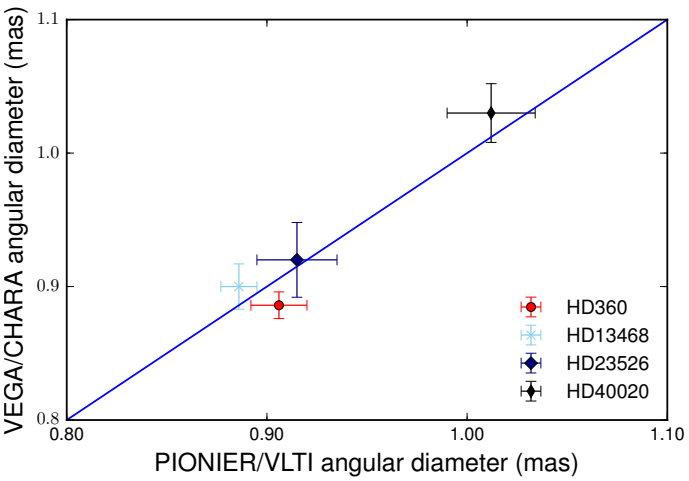

Fig. 1. Angular diameters derived from VEGA/CHARA compared to those from PIONIER/VLTI. The blue line marks the 1:1 relation.

3. Calibrating the surface brightness relation

The surface brightness of a star is linked to its visual intrinsic dereddened magnitude $m_{\rm V_0}$ and its limb-darkened angular diameter $\theta_{\rm LD}$ by the following relation: $S_{\rm V} = m_{\rm V_0} + 5 \log \theta_{LD}$. In order to derive $m_{\rm V_0}$, we first selected the apparent $m_{\rm V}$ magnitude from the main Hipparcos and Tycho catalog (ESA 1997) expressed in the Johnson system (Johnson et al. 1966). For the dereddening of these magnitudes, we used $m_{\rm V_0} = m_{\rm V} - A_V$, where A_V is either taken directly from Pietrzyński et al. (2019) for the four targets we have in common or based on Stilism[2] (Lallement et al. 2014; Capitanio et al. 2017). Pietrzyński et al. (2019) used the 2D reddening maps of Schlegel et al. (1998) and Schlafly & Finkbeiner (2011). These maps give a total extinction in a given line of sight, while the reddening to a given star is only a small fraction of it. To calculate this fraction, they used a simple exponential model of dust distribution in the Milky Way, the Hipparcos parallaxes, and the local extinction-free bubble radius of 40 pc (Suchomska et al. 2015). Stilism is a 3D maps of the Galactic interstellar medium based on a combination of various methods and databases. The extinction we used for each star in our sample is indicated in Tab. 3, and the effect of these extinctions on the SBCR is discussed in the next section. Then the color follows with $(V-K)_0 = (V-K) - A_V - A_K$, where $A_{\rm K} = 0.089 A_{\rm V}$ (Nishiyama et al. 2009). The $m_{\rm K}$ magnitudes are homogeneously derived from Laney et al. (2012). The $S_{\rm V}$ values are given in Table 3.

[2] `https://stilism.obspm.fr/`

Table 3. Angular diameters obtained with VEGA/CHARA and the corresponding surface brightnesses. For each star, we consider an uncertainty of 0.01 magnitude for $m_{\rm V}$ and $m_{\rm K}$ (Laney et al. 2012). The angular diameter of stars marked with an asterisk is based on PIONIER/VLTI observations provided in the extended data Table 2 of Pietrzyński et al. (2019). This is reported here in the last column.

Star	$m_{\rm V}$ [mag]	$m_{\rm K}$ [mag]	$A_{\rm V}$ [mag]	$(V-K)_0$ [mag]	$\theta_{\rm UD}{}^{\pm\sigma_{\rm stat}}_{\pm\sigma_{\rm syst}}$ [mas]	$\chi^2_{\rm red}$	$u_{[710]}$	$\theta_{\rm LD}{}^{\pm\sigma_{\rm stat}}_{\pm\sigma_{\rm syst}}$ [mas]	$S_{\rm v}{}^{\pm\sigma_{\rm stat}}_{\pm\sigma_{\rm syst}}$ [mag]	$\theta_{\rm LD}{}^{\pm\sigma_{\rm stat}}_{\rm PIONIER}$ [mas]
HD11037	$5.910_{\pm0.010}$	$3.666_{\pm0.010}$	0.031	2.216	$0.841^{\pm0.018}_{\pm0.002}$	1.3	0.631	$0.890^{\pm0.019}_{\pm0.002}$	$5.626^{\pm0.047}_{\pm0.011}$	
HD13468*	$5.940_{\pm0.010}$	$3.666_{\pm0.010}$	0.028	2.248	$0.851^{\pm0.016}_{\pm0.002}$	1.6	0.628	$0.900^{\pm0.017}_{\pm0.002}$	$5.683^{\pm0.042}_{\pm0.011}$	$0.886^{\pm0.009}$
HD22798	$6.220_{\pm0.010}$	$3.880_{\pm0.010}$	0.012	2.329	$0.749^{\pm0.020}_{\pm0.002}$	2.9	0.631	$0.792^{\pm0.021}_{\pm0.002}$	$5.701^{\pm0.058}_{\pm0.011}$	
HD23526*	$5.910_{\pm0.010}$	$3.634_{\pm0.010}$	0.053	2.228	$0.869^{\pm0.025}_{\pm0.001}$	0.6	0.631	$0.920^{\pm0.027}_{\pm0.001}$	$5.676^{\pm0.064}_{\pm0.010}$	$0.915^{\pm0.020}$
HD360*	$5.990_{\pm0.010}$	$3.653_{\pm0.010}$	0.028	2.311	$0.835^{\pm0.009}_{\pm0.002}$	0.5	0.658	$0.886^{\pm0.010}_{\pm0.002}$	$5.699^{\pm0.026}_{\pm0.011}$	$0.906^{\pm0.014}$
HD40020*	$5.890_{\pm0.010}$	$3.419_{\pm0.010}$	0.040	2.434	$0.969^{\pm0.024}_{\pm0.005}$	0.4	0.668	$1.030^{\pm0.025}_{\pm0.005}$	$5.913^{\pm0.053}_{\pm0.014}$	$1.012^{\pm0.022}$
HD43023	$5.830_{\pm0.010}$	$3.704_{\pm0.010}$	0.003	2.123	$0.796^{\pm0.012}_{\pm0.001}$	1.1	0.631	$0.842^{\pm0.014}_{\pm0.001}$	$5.453^{\pm0.037}_{\pm0.010}$	
HD5268	$6.150_{\pm0.010}$	$3.910_{\pm0.010}$	0.043	2.200	$0.725^{\pm0.033}_{\pm0.005}$	0.5	0.628	$0.767^{\pm0.035}_{\pm0.005}$	$5.530^{\pm0.099}_{\pm0.017}$	

Table 4. Fundamental parameters of the stars in our sample based on spectroscopy and combined with photometry for stars in Luck & Heiter (2007).

Star	Sp. Type	$T_{\rm eff}$ [K]	$\log g$	Z	V_t [km s^{-1}]	round $T_{\rm eff}$ [K]	round $\log g$	round Z	round V_t [km s^{-1}]	references
HD11037	K0III	4976	2.85	-0.10	1.5	5000	3.0	0.0	1.0	Luck & Heiter (2007)
HD13468	K0III	4940	2.59	-0.17	1.0	5000	2.5	0.0	1.0	Jones et al. (2011)
HD22798	K0III	4905	2.99	0.24	1.0	5000	3.0	0.2	1.0	Soubiran et al. (2008)
HD23526	G9III	4935	2.81	-0.12	1.0	5000	3.0	0.0	1.0	Luck & Heiter (2007)
HD360	G9III	4741	2.73	-0.05	1.3	4750	3.0	0.0	1.0	Liu et al. (2007)
HD40020	K2III	4752	2.67	0.17	2.0	4750	2.5	0.2	2.0	Luck & Heiter (2007)
HD43023	K0III	5105	3.08	-0.06	1.5	5000	3.0	0.0	1.0	Luck & Heiter (2007)
HD5268	G8III	4904	2.35	-0.57	1.0	5000	2.5	0.0	1.0	Jones et al. (2011)

In order to fit our SBCR, we used the same formalism as Pietrzyński et al. (2019),

$$S_{\rm V} = \alpha[(V-K)_0 - 2.405] + \beta, \quad (1)$$

where α and β are the slope and zero-point of the relation, respectively. The value 2.405 is the average color of the stars that were used to built the SBCR in Pietrzyński et al. (2019). We kept this value in our fit to allow a direct comparison. We first fit both parameters and then assumed the slope from the SBCR of Pietrzyński et al. (2019). The statistical uncertainty on the magnitudes $m_{\rm V}$ and $m_{\rm K}$, on the extinction $A_{\rm V}$, and on the surface brightness $S_{\rm v}$ were taking into account in the fitting process. Results are summarized in Tab. 5. We obtain very similar results when we fit one or two parameters (1.7% difference on the slope and 0.05% on the zero-point), as shown by Fig. 2. The SBCRs from Kervella et al. (2004b), Di Benedetto (2005), and Challouf et al. (2014) are shown for comparison.

4. Discussion

Our relation has an rms of 0.04 magnitude (Tab. 5) and is consistent with all other SBCRs presented in Fig. 2, except for that of Challouf et al. (2014), in particular for a $(V-K)$ color larger than 2.3 magnitude. This is explained by the fact that the relation by Challouf et al. (2014) is nonlinear, was based on 132 stars of all classes, and was fit over a very wide range of color from early to late types. We note that this relation was dedicated to O, B, A stars.

Conversely, the relation by Pietrzyński et al. (2019), which has an rms of 0.018 magnitude, is consistent with all SBCRs (except for that of Challouf et al. (2014)), including the SBCR in this work. These relations are indeed consistent (within 1%), even though different methods were used. The relation by Pietrzyński et al. (2019) is based on the observation of 48 giant stars in the H band with the PIONIER/VLTI (Gallenne et al. 2018), while the relation by Kervella et al. (2004b) is based on a set of angular diameters of dwarfs and subgiant stars derived from different optical and infrared interferometers: NPOI, NII (Narrabri Intensity Interferometer, Hanbury Brown et al. (1967)), Mark III (Shao et al. 1988), PTI (Palomar Testbed Interferometer, Colavita et al. (1999)), and VINCI (Kervella et al. 2004a). The relation by Di Benedetto (2005) is based on the NPOI (Navy Prototype Optical Interferometer, Armstrong et al. (1998)) observations by Nordgren et al. (2001) of 24 giants and three dwarfs obtained in the optical domains (wavelength of reference of 740 nm). Thus, following Salsi et al. (2020, in preparation), who found a different SBCR depending on the spectral type and class of the stars, we can consistently compare the relations by Pietrzyński et al. (2019), Di Benedetto (2005) and ours, which are all based on giants. On the color range considered, the relation in this work (rms of 0.039 mag) is consistent with the relation

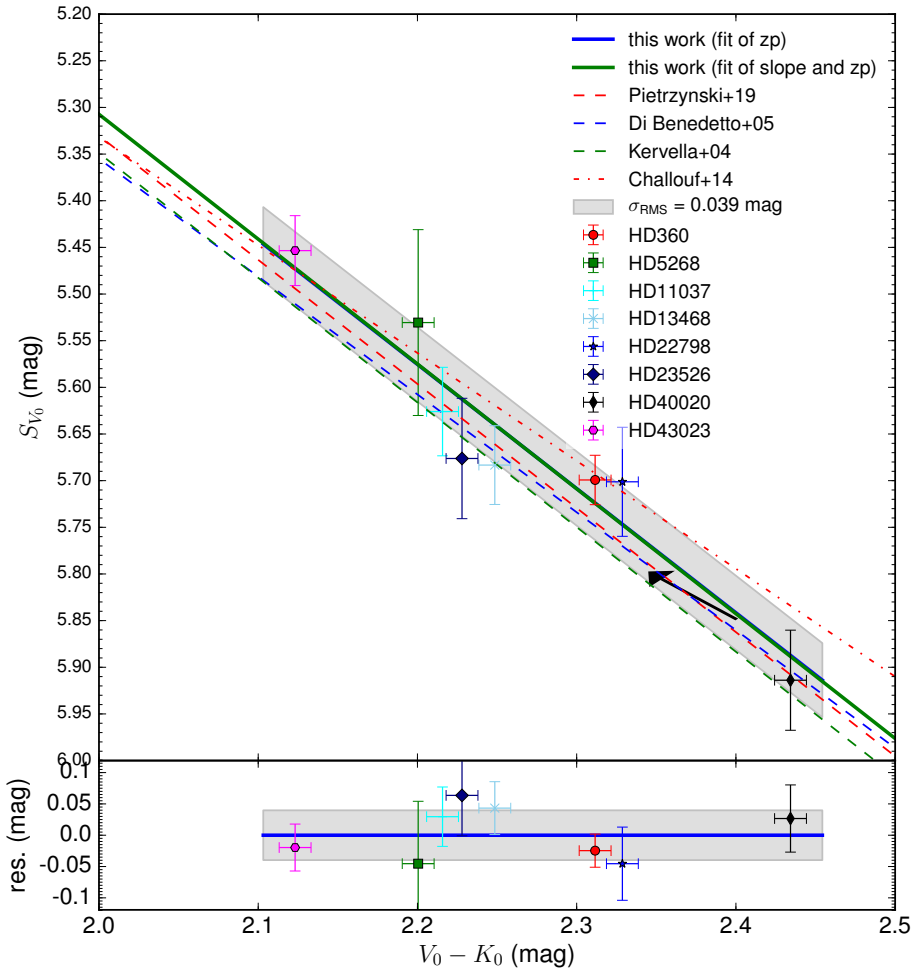

Fig. 2. Surface brightness – color relation derived from VEGA/CHARA data of eight late-type stars with a homogenous set of infrared photometry (Laney et al. 2012). The black arrow shows the effect of an additional extinction of 0.1 magnitude on a measurement. The gray zone corresponds to the rms.

Table 5. Fit of the SBCR. Slope and zero-point of the SBCR were first fit using Eq. 1. We then assumed the slope from the SBCR of Pietrzyński et al. (2019) (indicated by an asterisk). The reduced χ^2 is 0.4 in both cases.

Reference	β	α	rms
Pietrzynski et al. (2018)	$5.869_{\pm 0.003}$	$1.330_{\pm 0.017}$	0.018
this work	$5.849_{\pm 0.027}$	$1.338_{\pm 0.160}$	0.039
this work	$5.848_{\pm 0.013}$	$1.330^{\star}$	0.039

by Di Benedetto (2005) (rms of 0.04 mag) and with the relation by Pietrzyński et al. (2019) (rms of 0.018 mag).

It is well known that the extinction has a negligible effect on the SBCR because the color and surface brightness are sensitive to it in almost the same way. The only difference comes from the extinction in K, which is about 10% of the extinction in V. Adding an extinction of 0.1 magnitude on a measurement, for instance, results in a brighter color of the star of about 0.054 magnitude, and similarly, in a brighter surface-brightness of 0.05 magnitude. In order to quantify the effect of extinction on the SBCR, we arbitrarily changed the absorption (A_V) of all stars in our sample. We find that a higher extinction of 0.1 magnitude results in an increase in zero-point of the SBCR by 0.045 magnitude, which corresponds to the rms of our SBCR. This offset becomes 0.048 magnitude when we use the older relationship $A_K = 0.114 A_V$ from Cardelli et al. (1989) instead of the relation we considered in Sect. 3 ($A_K = 0.089 A_V$) from Nishiyama et al. (2009). This means that even if the A_V values of the star in the sample were all under-estimated by 0.1 magnitude (which is highly unlikely), our SBCR would still be consistent with the SBCR by Pietrzyński et al. (2019).

5. Conclusion

We observed eight red clump stars (late-type giants) with the VEGA/CHARA instrument and derived their angular diameters with an average precision of 2.4%. By combining these diameters with a homogeneous set of infrared photometry (Laney et al. 2012), we derived the slope and zero-point of the SBCR with a residual dispersion of 0.04 magnitude (or 1.8% precision in terms of angular diameter). The zero-points of the SBCR derived in the H band and in the visible domain are consistent at the 0.4% level (or 0.5σ). The an-

gular diameters of four stars in our sample are consistent with those found by VLTI/PIONIER, which shows that the systematics of both instruments are under control It also indicates that it is possible to combine interferometric measurements in different bands when the SBCR is calibrated. All these results confirm the recent claim of a 1% precision and accuracy on the LMC distance by Pietrzyński et al. (2019).

Acknowledgements. We acknowledge M. Schultheis for fruitful discussions about the extinction of stars. This research has made use of the SIMBAD and VIZIER[3] databases at CDS, Strasbourg (France) and of electronic bibliography maintained by the NASA/ADS system. This research has made use of the Jean-Marie Mariotti Center `LITpro` service co-developped by CRAL, IPAG and LAGRANGE[4]. This research has made use of the Jean-Marie Mariotti Center `Aspro` service [5]. This work was supported by the "Programme National de Physique Stellaire (PNPS) of CNRS/INSU co-funded by CEA and CNES. This work was supported by the "Action Spécifique pour la Haute Résolution Angulaire (ASHRA) of CNRS/INSU co-funded by CNES. The CHARA Array is funded by the National Science Foundation through NSF grants AST-0606958 and AST-0908253 and by Georgia State University through the College of Arts and Sciences, as well as the W. M. Keck Foundation. R.L. has received funding from the European Union's Horizon 2020 research and innovation programme under the Marie Sklodowska-Curie grant agreement n. 664931. W.G. and G.P. gratefully acknowledge financial support for this work from the BASAL Centro de Astrofisica y Tecnologias Afines (CATA) AFB-170002. We acknowledge financial support for this work from ECOS-CONICYT grant C13U01. The authors acknowledge the support of the FrenchAgence Nationale de la Recherche (ANR), under grant ANR-15-CE31-0012-01 (project UnlockCepheids). Support from the Polish National ScienceCentre grants MAESTRO UMO-2017/26/A/ST9/00446 and from the IdPII 2015 0002 64 grant of the Polish Ministry of Science and Higher Education is also acknowledged. The research leading to these results has received funding from the European Re-search Council (ERC) under the European Unions Horizon 2020 research and innovation program (grant agreement No 695099).

References

Armstrong, J. T., Mozurkewich, D., Rickard, L. J., et al. 1998, ApJ, 496, 550
Bonneau, D., Clausse, J.-M., Delfosse, X., et al. 2006, A&A, 456, 789
Capitanio, L., Lallement, R., Vergely, J. L., Elyajouri, M., & Monreal-Ibero, A. 2017, A&A, 606, A65
Cardelli, J. A., Clayton, G. C., & Mathis, J. S. 1989, ApJ, 345, 245
Challouf, M., Nardetto, N., Mourard, D., et al. 2014, A&A, 570, A104
Claret, A. & Bloemen, S. 2011, A&A, 529, A75
Colavita, M. M., Wallace, J. K., Hines, B. E., et al. 1999, ApJ, 510, 505
Di Benedetto, G. P. 2005, MNRAS, 357, 174
ESA, ed. 1997, ESA Special Publication, Vol. 1200, The HIPPARCOS and TYCHO catalogues. Astrometric and photometric star catalogues derived from the ESA HIPPARCOS Space Astrometry Mission
Freedman, W. L. & Madore, B. F. 2010, ApJ, 719, 335
Gallenne, A., Pietrzyński, G., Graczyk, D., et al. 2018, A&A, 616, A68
Gieren, W., Storm, J., Barnes, III, T. G., et al. 2005, ApJ, 627, 224
Graczyk, D., Soszyński, I., Poleski, R., et al. 2011, Acta Astron., 61, 103
Hanbury Brown, R., Davis, J., & Allen, L. R. 1967, MNRAS, 137, 375
Hanbury Brown, R., Davis, J., Lake, R. J. W., & Thompson, R. J. 1974, MNRAS, 167, 475
Johnson, H. L., Mitchell, R. I., Iriarte, B., & Wisniewski, W. Z. 1966, Communications of the Lunar and Planetary Laboratory, 4, 99
Jones, M. I., Jenkins, J. S., Rojo, P., & Melo, C. H. F. 2011, A&A, 536, A71
Kervella, P., Ségransan, D., & Coudé du Foresto, V. 2004a, A&A, 425, 1161
Kervella, P., Thévenin, F., Di Folco, E., & Ségransan, D. 2004b, A&A, 426, 297
Komatsu, E., Smith, K. M., Dunkley, J., et al. 2011, ApJS, 192, 18
Lafrasse, S., Mella, G., Bonneau, D., et al. 2010, VizieR Online Data Catalog, 2300
Lallement, R., Vergely, J.-L., Valette, B., et al. 2014, A&A, 561, A91
Laney, C. D., Joner, M. D., & Pietrzyński, G. 2012, MNRAS, 419, 1637
Le Bouquin, J.-B., Berger, J.-P., Lazareff, B., et al. 2011, A&A, 535, A67
Ligi, R., Mourard, D., Nardetto, N., & Clausse, J.-M. 2013, Journal of Astronomical Instrumentation, 2, 40003
Liu, Y. J., Zhao, G., Shi, J. R., Pietrzyński, G., & Gieren, W. 2007, MNRAS, 382, 553
Luck, R. E. & Heiter, U. 2007, AJ, 133, 2464
Mourard, D., Bério, P., Perraut, K., et al. 2011, A&A, 531, A110
Mourard, D., Clausse, J. M., Marcotto, A., et al. 2009, A&A, 508, 1073
Neilson, H. R. & Lester, J. B. 2013a, A&A, 554, A98
Neilson, H. R. & Lester, J. B. 2013b, A&A, 556, A86
Nishiyama, S., Tamura, M., Hatano, H., et al. 2009, ApJ, 696, 1407
Nordgren, T. E., Sudol, J. J., & Mozurkewich, D. 2001, AJ, 122, 2707
Pawlak, M., Soszyński, I., Udalski, A., et al. 2016, Acta Astron., 66, 421
Pietrzyński, G., Graczyk, D., Gallenne, A., et al. 2019, Nature, 567, 200
Pietrzyński, G., Graczyk, D., Gieren, W., et al. 2013, Nature, 495, 76
Riess, A. G., Casertano, S., Yuan, W., Macri, L. M., & Scolnic, D. 2019, ApJ, 876, 85
Riess, A. G., Macri, L. M., Hoffmann, S. L., et al. 2016, ArXiv e-prints
Schaefer, B. E. 2008, AJ, 135, 112
Schlafly, E. F. & Finkbeiner, D. P. 2011, ApJ, 737, 103
Schlegel, D. J., Finkbeiner, D. P., & Davis, M. 1998, ApJ, 500, 525
Shao, M., Colavita, M. M., Hines, B. E., et al. 1988, ApJ, 327, 905
Soubiran, C., Bienaymé, O., Mishenina, T. V., & Kovtyukh, V. V. 2008, A&A, 480, 91
Sturmann, J., ten Brummelaar, T., Sturmann, L., & McAlister, H. A. 2010, in Society of Photo-Optical Instrumentation Engineers (SPIE) Conference Series, Vol. 7734, Society of Photo-Optical Instrumentation Engineers (SPIE) Conference Series, 3
Suchomska, K., Graczyk, D., Smolec, R., et al. 2015, MNRAS, 451, 651
Tallon-Bosc, I., Tallon, M., Thiébaut, E., et al. 2008, in Society of Photo-Optical Instrumentation Engineers (SPIE) Conference Series, Vol. 7013, Society of Photo-Optical Instrumentation Engineers (SPIE) Conference Series
ten Brummelaar, T. A., McAlister, H. A., Ridgway, S. T., et al. 2005, ApJ, 628, 453
Udalski, A., Szymanski, M. K., Soszynski, I., & Poleski, R. 2008, Acta Astron., 58, 69
Walker, E. S., Hachinger, S., Mazzali, P. A., et al. 2012, MNRAS, 427, 103

Appendix A: Plot of the CHARA/VEGA squared visibility measurements.

Appendix B: Table of the observing log

[3] Available at http://cdsweb.u- strasbg.fr/
[4] LITpro software available at http://www.jmmc.fr/litpro
[5] Available at http://www.jmmc.fr/aspro

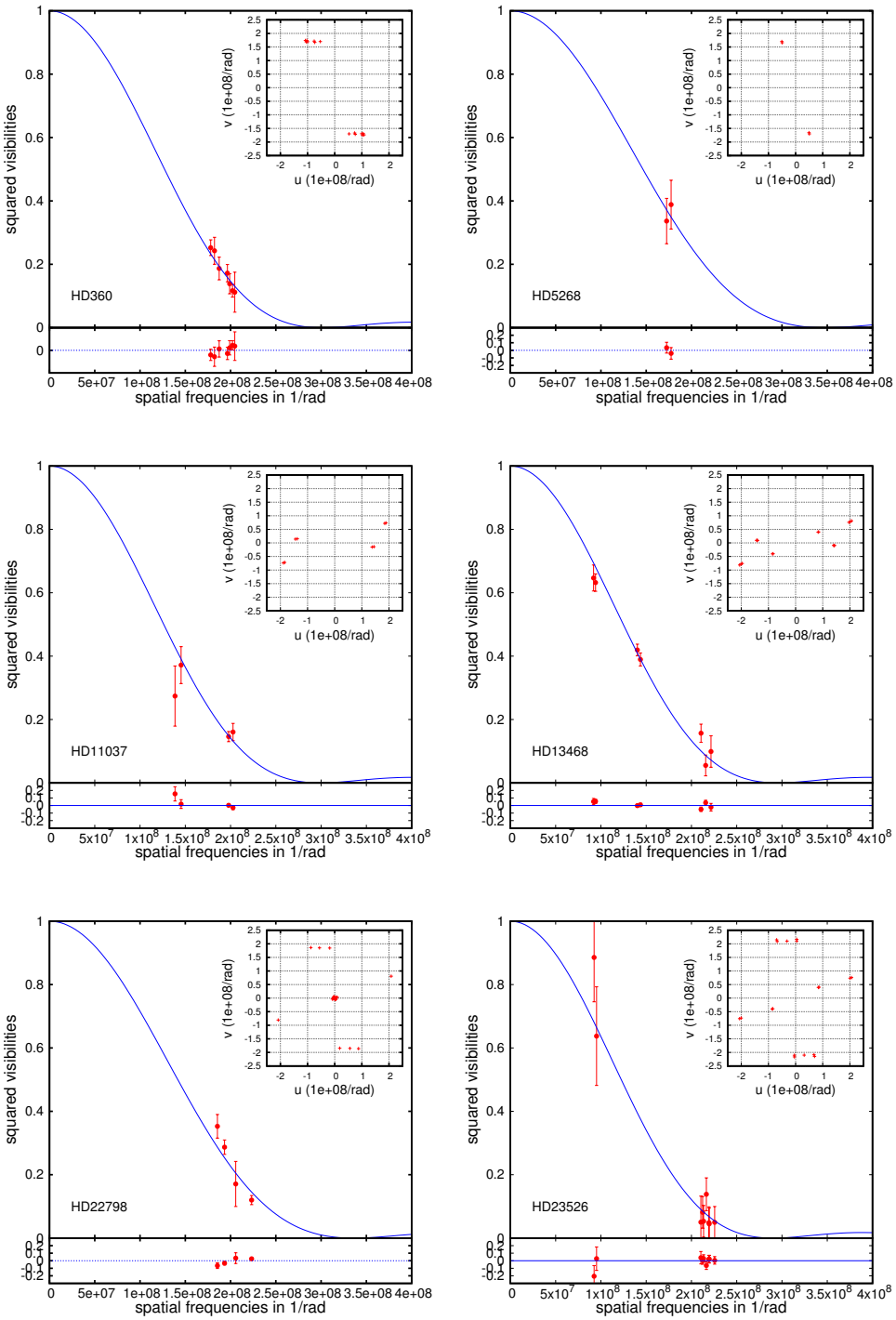

Fig. A.1. Squared visibility vs. spatial frequency for all stars in our sample with their corresponding statistical uncertainties (red dots). The solid blue lines indicate the best uniform-disk model obtained from the LITpro fitting software.

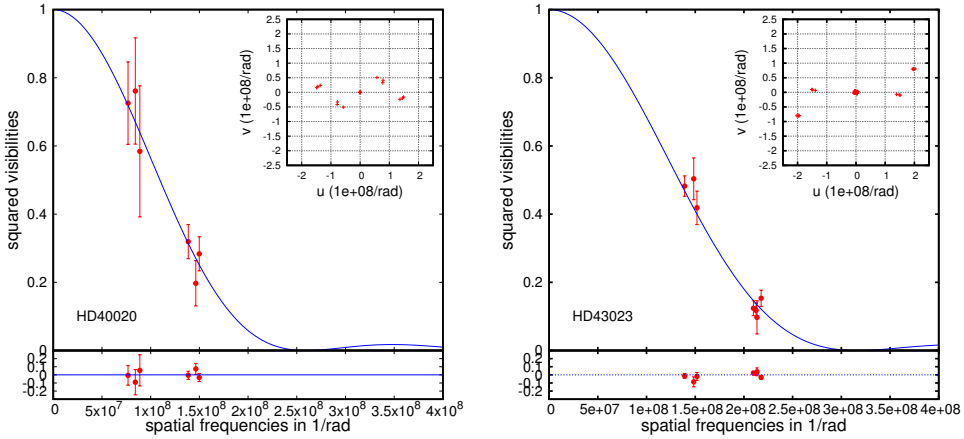

Fig. A.2. Squared visibility vs. spatial frequency for all stars in our sample with their corresponding statistical uncertainties (red dots). The solid blue lines indicate the best uniform-disk model obtained from the LITpro fitting software.

Table B.1. Observing log. The columns list the date, the reduced Julian date ($RJD = JD - 2400000$), the hour angle (HA), the minimum and maximum wavelengths over which the squared visibility is calculated, the projected baseline length Bp, and its orientation PA. The last column provides the calibrated squared visibility V^2 together with the statistic error on V^2 and the systematic error on V^2 (see text for details). Only the visibilities with a signal-to-noise ratio on the fringe peak higher than 1.7 were considered. The data are available on the Jean-Marie Mariotti Center `OiDB` service (Available at http://oidb.jmmc.fr).

	Date	RJD	HA	λ_{min}	λ_{max}	baseline	Bp	PA	$V^2_{cal \pm stat \pm syst}$
	[yyyy.mm.dd]	[days]	[h]	[nm]	[nm]		[m]	[deg]	
HD11037	2013.10.27	56592.686	-2.60	705	725	E2W2	144.95	-111.33	0.160 $\pm 0.027 \pm 0.003$
	2013.10.27	56592.686	-2.60	725	740	E2W2	144.95	-111.33	0.146 $\pm 0.016 \pm 0.002$
	2014.10.19	56949.773	-1.03	695	715	W1W2	97.74	-83.73	0.274 $\pm 0.095 \pm 0.002$
	2014.10.19	56949.793	-0.57	695	715	W1W2	102.47	-84.45	0.372 $\pm 0.058 \pm 0.003$
HD13468	2014.08.27	56896.906	-1.66	690	710	E1E2	65.85	-115.41	0.632 $\pm 0.027 \pm 0.003$
	2014.08.27	56896.906	-1.66	690	710	E2W2	155.13	-111.55	0.099 $\pm 0.050 \pm 0.003$
	2014.08.27	56896.945	-0.65	690	710	E1E2	64.31	-115.57	0.647 $\pm 0.041 \pm 0.003$
	2013.11.02	56598.777	-0.51	705	725	W1W2	102.72	93.72	0.389 $\pm 0.021 \pm 0.004$
	2013.11.02	56598.777	-0.51	705	725	W2E2	154.24	68.88	0.055 $\pm 0.033 \pm 0.001$
	2013.11.02	56598.777	-0.51	725	740	W1W2	102.72	93.72	0.419 $\pm 0.019 \pm 0.004$
	2013.11.02	56598.777	-0.51	725	740	W2E2	154.24	68.88	0.157 $\pm 0.029 \pm 0.004$
HD22798	2014.08.22	56892.002	-1.24	690	710	E2W2	156.25	-111.20	0.120 $\pm 0.014 \pm 0.002$
	2014.10.20	56950.816	-1.83	695	715	W2S2	130.75	-5.76	0.353 $\pm 0.037 \pm 0.004$
	2014.10.20	56950.853	-0.91	695	715	W2S2	136.30	-16.83	0.287 $\pm 0.023 \pm 0.004$
	2014.10.20	56950.890	-0.06	695	715	W2S2	145.01	-25.27	0.171 $\pm 0.071 \pm 0.002$
HD23526	2014.08.22	56891.974	-1.96	680	700	E2W2	151.53	-110.15	0.045 $\pm 0.050 \pm 0.001$
	2014.08.22	56891.974	-1.96	700	720	E2W2	151.53	-110.15	0.053 $\pm 0.050 \pm 0.001$
	2014.08.23	56892.985	-1.64	680	700	E1E2	65.66	64.98	0.637 $\pm 0.156 \pm 0.002$
	2014.08.23	56892.985	-1.64	700	720	E1E2	65.66	64.98	0.886 $\pm 0.140 \pm 0.002$
	2014.10.20	56950.797	-2.38	680	700	W2S2	149.38	-178.82	0.138 $\pm 0.052 \pm 0.002$
	2014.10.20	56950.797	-2.38	700	720	W2S2	149.38	-178.82	0.050 $\pm 0.082 \pm 0.001$
	2014.10.20	56950.834	-1.51	700	720	W2S2	150.78	171.40	0.081 $\pm 0.050 \pm 0.001$
	2014.10.20	56950.872	0.59	680	700	W2S2	155.72	161.98	0.050 $\pm 0.050 \pm 0.001$
	2014.10.20	56950.872	0.59	700	720	W2S2	155.72	161.98	0.049 $\pm 0.050 \pm 0.001$
HD360	2013.08.26	56530.922	0.55	695	715	W2S2	144.26	-31.84	0.112 $\pm 0.063 \pm 0.002$
	2013.08.26	56530.922	0.55	715	735	W2S2	144.26	-31.84	0.138 $\pm 0.032 \pm 0.002$
	2013.07.24	56497.945	-1.00	690	710	W2S2	124.66	-17.34	0.252 $\pm 0.025 \pm 0.006$
	2013.07.24	56497.971	-0.41	690	710	W2S2	131.20	-23.79	0.187 $\pm 0.036 \pm 0.004$
	2013.07.24	56497.971	-0.41	710	730	W2S2	131.20	-23.79	0.243 $\pm 0.043 \pm 0.005$
	2013.07.24	56498.003	0.35	690	710	W2S2	141.49	-30.45	0.117 $\pm 0.020 \pm 0.003$
	2013.07.24	56498.003	0.35	710	730	W2S2	141.49	-30.45	0.172 $\pm 0.027 \pm 0.005$
HD40020	2013.10.27	56592.860	-2.63	725	745	E1E2	61.90	67.00	0.761 $\pm 0.156 \pm 0.002$
	2013.11.26	56622.863	0.59	725	745	E1E2	65.35	62.21	0.584 $\pm 0.192 \pm 0.006$
	2013.11.26	56622.955	1.57	705	725	E1E2	54.87	48.71	0.726 $\pm 0.121 \pm 0.008$
	2014.10.22	56952.938	-1.05	700	720	W1W2	98.39	-80.11	0.319 $\pm 0.050 \pm 0.010$
	2014.10.22	56952.962	0.45	700	720	W1W2	103.90	-82.36	0.197 $\pm 0.067 \pm 0.006$
	2014.10.23	56953.976	0.04	700	720	W1W2	106.40	-83.77	0.284 $\pm 0.050 \pm 0.007$
HD43023	2013.10.26	56591.903	-1.98	710	725	E2W2	153.65	-112.31	0.097 $\pm 0.049 \pm 0.001$
	2013.10.26	56591.903	-1.98	725	740	E2W2	153.65	-112.31	0.124 $\pm 0.022 \pm 0.001$
	2013.10.26	56591.919	-1.59	705	725	E2W2	155.62	-111.65	0.153 $\pm 0.024 \pm 0.002$
	2013.10.26	56591.919	-1.59	725	740	E2W2	155.62	-111.65	0.118 $\pm 0.021 \pm 0.001$
	2014.10.16	56947.000	-0.25	695	715	W1W2	104.65	-86.71	0.504 $\pm 0.061 \pm 0.006$
	2014.10.16	56947.019	0.19	695	715	W1W2	106.99	-86.35	0.419 $\pm 0.049 \pm 0.005$
	2014.10.18	56948.965	-0.96	695	715	W1W2	98.08	-87.20	0.482 $\pm 0.030 \pm 0.004$
HD5268	2013.07.28	56501.961	-1.05	690	710	W2S2	124.28	163.39	0.388 $\pm 0.077 \pm 0.009$
	2013.07.28	56501.961	-1.05	710	730	W2S2	124.28	163.39	0.336 $\pm 0.072 \pm 0.008$